ACS APPLIED MATERIALS & INTERFACES

Research Article

www.acsami.org

Coating and Enhanced Photocurrent of Vertically Aligned Zinc Oxide Nanowire Arrays with Metal Sulfide Materials

Michael Volokh,[†] Mahmud Diab,[†] Osnat Magen,[‡] Ilan Jen-La Plante,[†] Kobi Flomin,[†] Pazit Rukenstein,[†] Nir Tessler,[‡] and Taleb Mokari*[,†]

[†]Department of Chemistry and Ilse Katz Institute for Nanoscale Science and Technology, Ben-Gurion University of the Negev, Beer-Sheva 8410501, Israel

[‡]The Sarah and Moshe Zisapel Nanoelectronic Center, Electrical Engineering Department, Technion-Israel Institute of Technology, Haifa 3200003, Israel

Supporting Information

ABSTRACT: Hybrid nanostructures combining zinc oxide (ZnO) and a metal sulfide (MS) semiconductor are highly important for energy-related applications. Controlled filling and coating of vertically aligned ZnO nanowire arrays with different MS materials was achieved via the thermal decomposition approach of single-source precursors in the gas phase by using a simple atmospheric-pressure chemical vapor deposition system. Using different precursors allowed us to synthesize multicomponent structures such as nanowires coated with alloy shell or multishell structures. Herein, we present the synthesis and structural characterization of the different structures, as well as an electrochemical characterization and a photovoltaic response of the ZnO−CdS system, in which the resulting photocurrent upon illumination indicates charge separation at the interface.

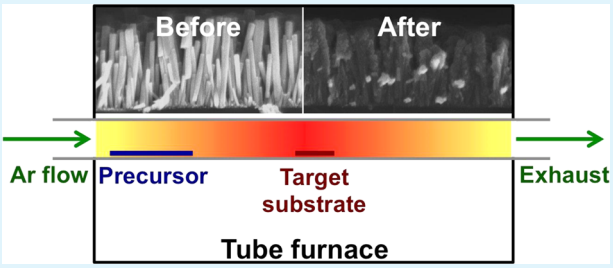

KEYWORDS: *nanowires, chemical vapor deposition, metal sulfides, single-source precursors, hybrid nanostructure*

INTRODUCTION

Hybrid nanostructures incorporating different semiconductors will be of paramount importance in many future energy-related applications such as photovoltaics,[1−3] water splitting,[4−7] catalysis,[8] batteries,[9] and nanogenerators.[10] In this work, we describe a synthetic method that combines ZnO nanowire (NW) templates with metal sulfide shells to create hybrid nanostructures. Such structures can be used not only for the applications mentioned above but also for other purposes, e.g., ultraviolet detectors,[11] gas sensors,[12] and devices for photoinactivation of bacteria.[13]

Metal sulfide films on flat substrates have been previously grown via metal−organic chemical vapor deposition (MOCVD) using two gas-phase precursors. Alternatively, aerosol-assisted chemical vapor deposition (AACVD) or low-pressure chemical vapor deposition (LPCVD) using single-source molecular precursors (SSP) have been used for this purpose.[14−18] Specifically, metal bis(diethyldithiocarbamate) [$M(dtcEt_2)_2$] SSPs were used to prepare thin films of CdS,[19,20] ZnS,[19] PbS,[20] and CuS[21] on flat substrates.

The advantage of using SSPs is their stability over time under ambient conditions, and the relatively low temperatures needed for the reaction. The additional benefit is that the reaction system is simpler than MOCVD and does not use hazardous or pyrophoric materials such as dimethylzinc or hydrogen sulfide. We use the SSP approach at atmospheric pressure to create high-quality metal sulfide coatings. Additional benefits of using the $M(dtcEt_2)_2$ family of materials include their simple and cheap preparation in water, their easy processing, and their well-known physical properties.[22,23]

These qualities facilitate the use of $M(dtcEt_2)_2$ SSPs for the synthesis of different metal sulfides also in the solution phase, such as spherical nanocrystals (NCs),[24,25] NWs,[25,26] and hybrid structures.[27] In the gas phase, NWs were synthesized via the vapor−liquid−solid (VLS) mechanism,[28] but hybrid structures of NWs and metal sulfides were reported either by using multiple precursors[29,30] or by preparing them in a one-step thermal evaporation.[31]

As was discussed earlier, heterojunctions between ZnO and metal sulfides are frequently used for different applications. Most of these nanostructures are achieved by deposition from a solution using various NC techniques such as chemical bath deposition (CBD),[3] electrodeposition,[32] successive ionic layer adsorption and reaction (SILAR),[33] spin-coating *ex situ* synthesized NCs,[34] etc.

To create efficient devices, which rely on charge separation across the heterojunction, the interface should be free of defects and the crystal orientation between the two materials should match. For example, in a hexagonal CdS crystal, the effective hole mass (m_h*) in the longitudinal direction is ∼7 times larger

Received: May 14, 2014
Accepted: August 8, 2014
Published: August 18, 2014

than in the transverse direction. Because the mobility and diffusion coefficients are inversely proportional to the effective mass, a hole can travel in the {110} direction much better than in the {001} direction,[35] which leads to a better conduction of holes perpendicular to the *c*-axis of CdS.

To the best of our knowledge, this is the first time that gas-phase decomposition of SSPs has been used to form hybrid structures of ZnO NWs covered with a varying thickness of a metal sulfide shell. We have chosen a ZnO−CdS model system to perform a complete characterization. We also demonstrated the growth of more complex systems, in which the ZnO NWs are coated with $Cd_xZn_{1-x}S$ with different compositions or a multishell structure like a ZnO−CdS−ZnS core−shell−shell system. In all these systems, we observed a preferential orientation between the decorating NCs and the ZnO NW. Furthermore, our method can be expanded to other metal sulfide shells (ZnS, NiS, and PbS) by changing the metal center in the $M(dtcEt_2)_2$ SSP and choosing the correct decomposition temperature.

EXPERIMENTAL SECTION

Materials. All solvents and reagents were purchased from Sigma-Aldrich, Alfa-Aesar, or Strem Chemicals and used without further purification. Deionized (DI) water was purified using a Millipore Direct-Q system (18.2 MΩ cm resistivity).

Substrates. Glass (1.25 cm × 2.5 cm), tin-doped indium oxide (ITO)-covered glass (Delta Technologies; R_s = 15−25 Ω), or polished Si(100) was cleaned using subsequent 15 min sonications in acetone, methanol, and 2-propanol.

Zinc Oxide Nanowire Arrays. Vertically aligned ZnO nanowire arrays were grown on cleaned substrates using a two-step method, slightly modified from the previously published approach.[36] Briefly, in the first step, a ZnO "seed layer" is formed, and in the second step, NWs are grown. Two seeding cycles were performed, each consisting of (a) three applications of 36 μL of a 9 mM solution of zinc acetate dihydrate [98% $Zn(II)ac_2{\cdot}2H_2O$] in anhydrous ethanol (99.9%), followed by an ethanol rinse, and (b) calcination at 315 °C for 30 min under air.

For NW growth, 20 mL glass vials were filled with 12 mL of an aqueous solution of 22 mM zinc acetate dihydrate and 28 mM hexamethylenetetramine (99% $C_6H_{12}N_4$) in DI water. The vials were heated to 85 °C, and the substrates were inserted into the unstirred vials. After a reaction time of 20−100 min (depending on the desired NW array height of ∼200−800 nm), the substrates were rinsed with DI water and calcined under air at 315 °C.

Filling and Coating of the ZnO NW Arrays with Metal Sulfide Materials. The home-built CVD system consists of a tube furnace (Thermo Scientific Lindberg Blue M Mini-Mite) with a 1 in. quartz tube. Both sides of the quartz tube are connected to a $^1/_4$ in. SS tube using an adapter. Argon gas (99.99%) is connected through a 65 mm flow meter (AALBORG) to one of the tube's sides. In a typical reaction, ∼0.75 g of the SSP was placed in a ceramic boat upstream of the substrates, which were placed in the middle of the furnace, where the temperature is measured. At first, an ∼125 sccm Ar flow was used for purging at room temperature, followed by purging for 30 min at 130 °C to eliminate oxygen and adsorbed water in the tube. During the film growth, the carrier gas flow rate is decreased to ∼23 sccm. The furnace temperature (T_{SP}) was set to 265−290 °C, which is the temperature of decomposition above the substrates. The temperature upstream, where the precursor boat is placed, is lower but sufficient to volatilize the precursor (∼240 °C); see Table S1 of the Supporting Information for details depending on the metal sulfide material and Figure S1 of the Supporting Information for the thermal gravimetric analysis (TGA) of the SSPs.

Syntheses of Single-Source Molecular Precursors. Metal bis(diethyldithiocarbamate)s $\{M(II)[S_2CN(C_2H_5)_2]_2\}$, where M = Cd, Zn, Ni, or Pb, were synthesized on the basis of a previously published method.[37] Briefly, 5 mmol of soluble metal salt [98% $Cd(II)ac_2{\cdot}2H_2O$, 98% $Zn(II)ac_2{\cdot}2H_2O$, 98% $Ni(II)ac_2{\cdot}4H_2O$, or 99% $Pb(II)ac_2{\cdot}3H_2O$] and 10 mmol of sodium diethyldithiocarbamate [99% $NaS_2CN(C_2H_5)_2$] were dissolved separately in DI water. Mixing the two solutions formed the product, which was filtered and dried for 2 h. The SSP precipitate was dissolved in hot chloroform (∼45 °C) and recrystallized by being cooled to 0 °C. The recrystallized SSP was dried at room temperature before further use.

Characterization. Scanning electron microscopy (SEM) and transmission electron microscopy (TEM) images were recorded using a JEOL JSM-7400F high-resolution scanning electron microscope operated at 3 kV and a FEI Tecnai T-12 G^2 TWIN transmission electron microscope operated at 120 kV, respectively. High-resolution transmission electron microscopy (HRTEM) analysis was conducted using a JEOL JEM-2100F instrument operated at 200 kV. Energy dispersive X-ray spectroscopy (EDS) was conducted using either the JSM-7400F high-resolution scanning electron microscope equipped with Thermo Scientific NORAN System SIX, or the JEM-2100F high-resolution transmission electron microscope in STEM mode equipped with a JEOL JED-2300T energy dispersive X-ray spectrometer. X-ray powder diffraction (XRD) data were collected from samples prepared on polished Si(100) substrates using a Philips 1050/70 diffractometer using Cu Kα radiation and operated at 40 kV and 28 mA. Absorbance spectra were measured using a Varian Cary 5000 UV−vis−NIR spectrophotometer. The electrochemical characterization was conducted in a three-electrode system in a 1 M KCl solution, using a VersaSTAT 3 potentiostat. An ITO covered with the characterized materials acted as the working electrode, Ag/AgCl in saturated KCl as the reference electrode, and a Pt wire as the counter electrode. Linear sweep voltammetry (LSV) was conducted by scanning at a rate of 0.03 V/s, from −0.6 to 0.4 V (1.4 V) under illumination (in the dark). A 365 nm LED (∼14 mW) was used as the illumination source. TGA was conducted using a Mettler Toledo TGA/SDTA 851e instrument under an 80 sccm N_2 flow from 25 to 400 °C at a rate of 5 °C min^{-1}.

RESULTS AND DISCUSSION

Hybrid ZnO−MS structures were synthesized by placing a substrate covered with ZnO NW arrays in the CVD tube, choosing the appropriate precursor, and performing the reaction as depicted in Scheme 1 (see the Experimental Section for details).

Scheme 1. Cartoon of the CVD Process

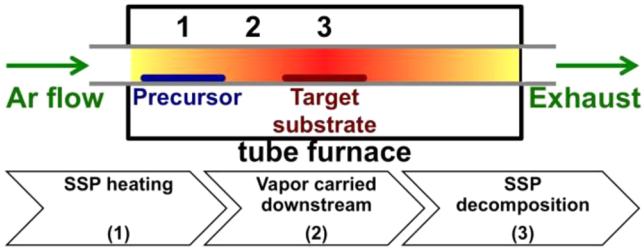

To achieve a controlled filling and coating of the NWs, the reaction was repeatedly performed for short ∼1 h cycles. Figure 1 and Figure S2 of the Supporting Information show SEM images of a typical coating growth of the ZnO NW arrays with CdS (cross section and top view, respectively). After the first cycle, the ZnO NWs are decorated with ∼10 nm CdS nanocrystals as seen in Figure 1b. Repeating the reaction leads to complete decoration, yielding a conformal shell (Figure 1c,d). Additional cycles result in filling of the gaps between the NWs (Figure 1e,f). After five cycles, the ZnO NW array is completely embedded in the CdS.

The gradual filling with CdS is also confirmed by measuring the absorption of the formed hybrid materials at different

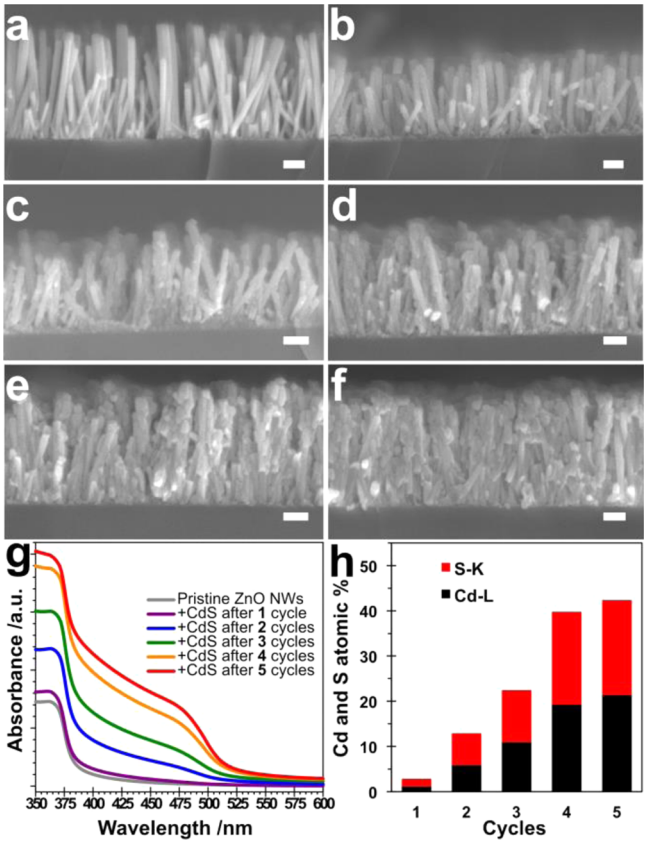

Figure 1. Gradual CdS filling of ZnO NWs. SEM cross section images of (a) ZnO NWs only. (b) One CdS CVD cycle. (b) Two CdS CVD cycles. (d) Three CdS CVD cycles. (e) Four CdS CVD cycles. (f) Five CdS CVD cycles. (g) UV–vis absorbance spectra of the different filling stages. (h) EDS atomic percentage of Cd and S out of the total quantified Zn, O, Cd, and S for the different cycles. All scale bars are 100 nm. Absorbance spectra were recorded for glass substrates; SEM and EDS were performed on Si substrates.

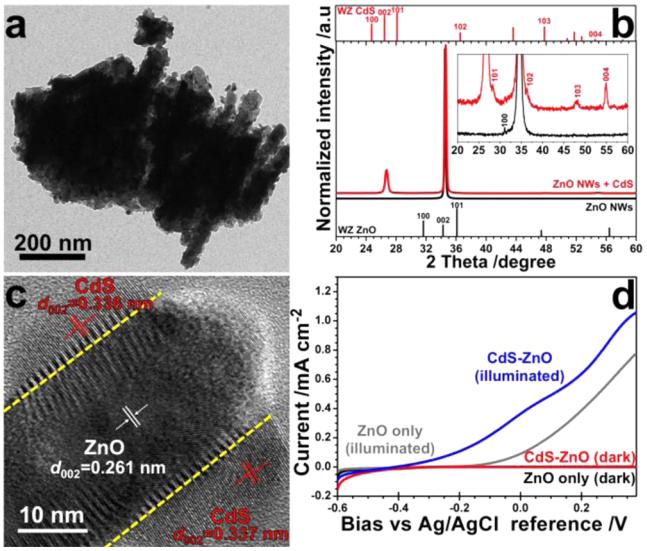

Figure 2. Characterization of CdS-coated ZnO NWs. (a) TEM image of CdS-coated ZnO NWs. (b) XRD patterns of pristine ZnO NWs (black) and CdS-coated NWs (red) were collected from Si substrates. The inset shows magnified patterns at low intensities. (c) HRTEM of an individual coated NW. (d) Linear sweep voltammetry of ITO/ZnO NWs and ITO/ZnO NW–CdS substrates, in the dark or under illumination (365 nm LED source) in an aqueous solution (1 M KCl acts as the supporting electrolyte).

thicknesses as presented in Figure 1g. The absorbance spectra show two band-edge absorbance peaks; the onset at ~380 nm corresponds to the band gap transition of ZnO,[38] and the onset at ~510 nm corresponds to the bulk band edge energy of CdS.[39] Furthermore, every additional cycle of SSP deposition increases both the absorbance of the CdS and the amount of Cd and S elements detected in the EDS analysis (Figure 1h). After the first cycle, the combined atomic contribution of Cd and S is <3 atom % but increases to >42 atom % after the fifth cycle. We tried to achieve similar results by conducting the experiment by using a single reaction cycle for longer times; however, it led to a conformal coating of the NW array (similar to the results in Figure 1c,d), and no complete filling was observed. Therefore, a multistep process (several cycles) is important for achieving a complete filling.

Characterization of the interface between the core and the shell was conducted on thin shell ZnO–CdS heterostructures. This hybrid material was produced by a single cycle of >2 h CVD. The low-magnification TEM image shows that the ZnO NWs are decorated with mostly quasi-elongated CdS nanocrystals with widths of ~5–10 nm and lengths of ~10–25 nm as presented in Figure 2a.

XRD analysis of the hybrid CdS–ZnO NWs is shown in Figure 2b. Plain ZnO NWs before (black pattern) and after the coating with CdS (red pattern) are shown. The strongest peak corresponds to the (002) planes of hexagonal wurtzite ZnO (JCPDS Card No. 36-1451). The next two strongest peaks in the CdS-coated NWs correspond to the (002) and (004) planes of hexagonal wurtzite CdS (wz-CdS) (JCPDS Card No. 41-1049), ~27° and ~55°, respectively. The relative intensities of these two peaks are much stronger than the powder diffraction values in the literature. The other significant peaks of a hexagonal crystallographic phase are much weaker, and the (100) peak is not observed. We attribute this result to the fact that there is a preferential orientation of the CdS crystals on the surface of the ZnO NWs. Further support for this observation is obtained by the HRTEM analysis as shown in Figure 2c. It can be clearly seen that ZnO NW and the CdS crystals are aligned with their *c*-axes. For all the measured hybrid structures, the *c*-axes of the decorating CdS nanocrystals and the ZnO NW correspond. Fast Fourier transform (FFT) of the CdS NCs on the ZnO NW confirms the hexagonal symmetry of the CdS and shows that the angle between the *c*-axes is between ~3° and 5°.

Elemental analysis of this NW was conducted via the transmission electron microscope using the EDS detector as presented in Figure S3 of the Supporting Information. The obtained atomic percentage results (Zn–K, 31.59%; O–K, 47.46%; Cd–L, 10.64%; S–K, 10.31%) correspond to the bulk EDS analysis conducted using the scanning electron microscope. An EDS line scan measurement of the ZnO–CdS core–shell NWs shows that the Zn and O are centered at the middle of the spectrum while the Cd and S are mainly located at the edges, as presented in Figure S4 of the Supporting Information. This result is evidence of the phase separation between the two materials.

To better verify the interface between the ZnO and the CdS, an electrochemical analysis was performed. This measurement can provide insight into the charge dynamics at the interface of this heterostructure. It has been shown that the interface between ZnO and CdS is type II where the energy band

alignment can facilitate charge separation.[3,13] A band alignment scheme for this system is presented as Figure S5 of the Supporting Information. Figure 2d presents a comparison between the electrochemical behavior of ZnO NWs with and without a CdS shell. These measurements were performed in an aqueous solution without using hole scavengers. Linear sweep voltammetry (LSV) shows that under illumination (365 nm), the onset was shifted to an ∼200 mV lower voltage for ZnO−CdS compared to that for ZnO, and higher photocurrents were measured. For example, the photocurrent ($j_{illuminated} - j_{dark}$) at 0 V bias was 0.09 mA cm^{-2} for plain ZnO NWs, while for the ZnO−CdS NWs, it was 0.32 mA cm^{-2}. In the dark, the addition of the CdS lowered the onset of the current by ∼300 mV (Figure S6 of the Supporting Information) compared to that of the plain ZnO. An additional LSV measurement with varying CdS shell thicknesses is presented in Figures S7 and S8 of the Supporting Information.

The measured current indicates that either holes oxidize the water or electrons are transferred through the ITO to the Pt counter electrode and reduce the water. It is well-established that direct oxidation of water at the photoanode's interface is slow.[40] Therefore, it is more likely that the main contribution to the current is electrons from both the CdS and the ZnO, which traveled through the NWs to the ITO substrate and then to the Pt wire counter electrode, which acts as the photocathode. This result supports the feasibility of this system for water splitting and indicates that this synthetic method is capable of forming type II core−shell heterostructures. Further confirmation of the potential of this system is presented in Figure S9 of the Supporting Information, where the heterostructure is incorporated in a photovoltaic device. The external quantum efficiency (EQE) peak coincides with the absorbance of the CdS, indicating that the CdS contributes to the photocurrent.

This coating method can be easily expanded to other metal sulfides such as ZnS, NiS, and PbS simply by changing the metal cation in the M(dtcEt$_2$)$_2$ SSP as shown in Figure S10 of the Supporting Information. Furthermore, our approach allows the growth of more complex hybrid nanostructures such as core−shell−shell and core−alloy shell systems. We have chosen to form a core−shell−shell ZnO−CdS−ZnS structure as shown in Figure 3.

Figure 3a shows the SEM image of the ZnO NW array filled with the two materials. The formation of the core−shell−shell structures is structurally verified by XRD (Figure 3b). The red pattern shows ZnO NWs coated only with wz-CdS. The (002) peak of CdS at ∼27° is the strongest, followed by the (101) peak at ∼28°. After the growth of the second shell of ZnS, the blue pattern was obtained. The comparison between the two patterns shows similar features, but the ratio between the (002) and (101) peaks significantly changes. We attribute this increase to the overlap between the CdS and ZnS peaks.

In this case, it is hard to distinguish between the two possible phases of ZnS because the reflections of the (101) planes of wz-CdS, the (111) plane of zinc-blende ZnS (zb-ZnS), and the (002) plane of wz-ZnS appear almost at the same 2θ value. When ZnO NWs are coated with only ZnS, an evident zb-ZnS pattern with a single strong (111) peak is measured, as in the black pattern (Figure 3b). Because the enhanced peak in the ZnO−CdS−ZnS system is at an angle slightly smaller than that of the zb-ZnS (111) peak in the ZnO−ZnS system (black pattern), it indicates either partial alloying at the interface between the materials or the formation of a thin wz-ZnS shell. Although the zinc-blende phase is more stable at room

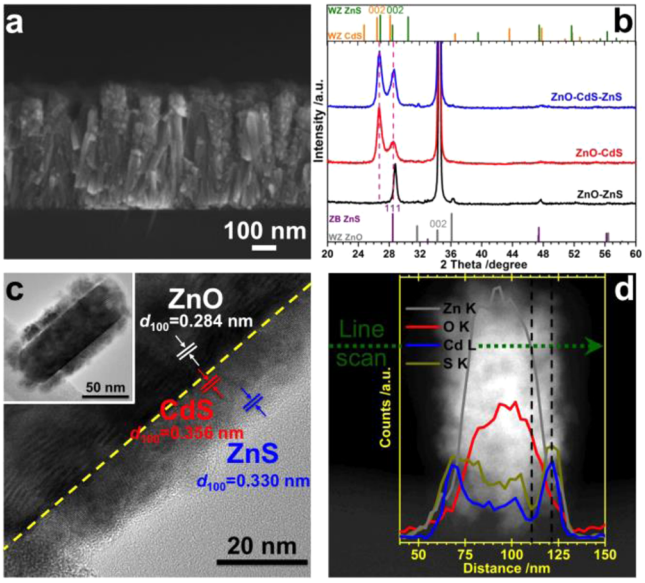

Figure 3. Characterization of a ZnO−CdS−ZnS system. (a) SEM cross section image. (b) XRD patterns of ZnO−ZnS, ZnO−CdS, and ZnO−CdS−ZnS systems. (c) HRTEM characterization. The inset shows a low-magnification image. (d) EDS line scan overlaid on an STEM image. SEM and XRD were performed on Si substrates.

temperature, it has been reported that small ZnS NCs can be formed as wz-ZnS.[41] Because the ZnS shell is grown directly on wz-CdS, a thin shell of wz-ZnS could be possible.

HRTEM analysis (Figure 3c) supports the presence of wurtzite structures of the three materials, as the measured lattice spacing of all three materials corresponds to the hexagonal (100) direction. However, we could not rule out a mixed-phase situation. An EDS line scan of the NW analyzed in Figure 3c is presented in Figure 3d. The black dashed lines indicate the approximate boundaries. At the first boundary, there is a strong increase in the detected amount of Cd and S (blue and olive lines, respectively). At the second boundary, the magnitude of the Zn signal increases (gray lines), which is accompanied by a decrease in that of Cd (blue lines). This measurement confirms the formation of a ZnO−CdS−ZnS core−shell−shell structure.

Another interesting structure that we succeeded in growing is the ZnO−Cd$_x$Zn$_{1-x}$S core−alloy shell NW. The possible polymorphs of CdS and ZnS have some resemblance as do the valences of their atoms. They can form solid solutions of Cd$_x$Zn$_{1-x}$S with x ranging from 0 to 1 in either the hexagonal (wz) or the cubic (zb) phase, depending on the temperature.[42] Via the simultaneous covolatilization of the two SSPs [Cd(dtcEt$_2$)$_2$ and Zn(dtcEt$_2$)$_2$] in the same reaction, a single solid solution phase of the alloy shell is formed on the ZnO NWs. Figure 4 shows two different compositions of Zn-rich (#1, x = 0.38) and Cd-rich (#2, x = 0.83) Cd$_x$Zn$_{1-x}$S alloy shells.

The SEM images of the Zn-rich phase (Figure 4a,b) show a thinner shell with better uniformity compared to that of the Cd-rich phase (Figure 4c,d). This is probably due to the smaller lattice mismatch between ZnS and ZnO relative to that of CdS. The normalized absorbance spectra (Figure 4e) show three peaks (pure CdS in black, Cd-rich solid solution in red, and Zn-rich solid solution in blue) relative to plain ZnO NWs (gray). As expected, the peaks are blue-shifted as the solid solution is more Zn-rich. The most noticeable difference between the

dx.doi.org/10.1021/am502976v | ACS Appl. Mater. Interfaces 2014, 6, 13594−13599

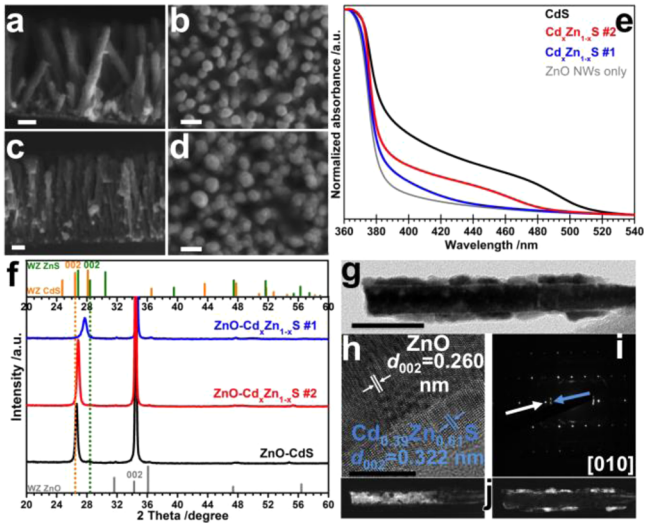

Figure 4. Characterization of two $Cd_xZn_{1-x}S$ solid solutions on ZnO NWs (#1 is Zn-rich, and #2 is Cd-rich). SEM images of sample #1: (a) cross section and (b) top view. SEM images of sample #2: (c) cross section and (d) top view. All scale bars are 100 nm. (e) Normalized absorbance spectra of the two solid solutions on ZnO NWs, with spectra of pure CdS and pristine ZnO NWs for comparison. (f) XRD patterns of the two solid solutions and pure CdS for comparison, all on ZnO NWs. (g) BF TEM image of a NW covered with $Cd_xZn_{1-x}S$ sample #1 (the scale bar is 50 nm). (h) HRTEM image, focused on the interface of $Cd_xZn_{1-x}S$ sample #1 (the scale bar is 10 nm). The measured lattice spacing (d_{002}) of 0.260 nm is of the ZnO core, and the d_{002} of 0.322 nm is of the $Cd_{0.39}Zn_{0.61}S$ shell. (i) SAED. White and blue arrows mark one of the ⟨002⟩ diffractions of ZnO and $Cd_xZn_{1-x}S$ sample #1, respectively. (j) DF images using the ⟨002⟩ reflections showing the ZnO core on the left and the $Cd_xZn_{1-x}S$ shell on the right. Absorbance spectra were taken from glass substrates; SEM and XRD analyses were performed on Si substrates.

samples is seen in the XRD patterns as shown in Figure 4f. The (002) peak of the $Cd_xZn_{1-x}S$ solid solution appears at higher angles with an increasing Zn content. By assuming a linear relationship (according to Vegard's law)[43] between the lattice spacing and the composition of the alloy, sample #1 (blue) fits the composition of $Cd_{0.38}Zn_{0.62}S$ and sample #2 (red) corresponds to $Cd_{0.83}Zn_{0.17}S$ (see Figure S11 of the Supporting Information).

To further confirm this analysis, Zn-rich sample #1 was analyzed using HRTEM. The bright-field (BF) image in Figure 4g shows a shell, which is more uniform than the shell with only CdS, as was also observed by the SEM images. HRTEM (Figure 4h) confirms the composition of the solid solution. The selected area electron diffraction (SAED) pattern (Figure 4i) presents a clear hexagonal symmetry in both the ZnO NW and the $Cd_xZn_{1-x}S$ shell. The calculated d spacing of the (002) and (100) reflections in the SAED confirms the formation of $Cd_{0.36}Zn_{0.64}S$, which is consistent with the XRD and HRTEM measurements. The dark-field (DF) images using the (002) reflections of the ZnO core (left image) and the $Cd_xZn_{1-x}S$ shell (right side) are shown in Figure 4j.

CONCLUSIONS

We have shown that a general and simple atmospheric-pressure CVD system utilizing cheap SSPs allows a controlled filling and coating of ZnO NW arrays at moderate temperatures. Complex structures or solid solutions can be formed and the composition tuned by a simple mixing of the SSPs. One of the main advantages of our method is the formation of a "clean" interface (free of structural defects) between the ZnO core and the CdS or the $Cd_xZn_{1-x}S$ shell, which would be useful in any energy application in which the charge separation is required.

ASSOCIATED CONTENT

Supporting Information

Table of detailed CVD parameters, TGA, top view SEM images of different filling stages of the ZnO−CdS system, analytical TEM (including EDS) characterization of the CdS−ZnO system, ZnO−CdS band alignment scheme, LSV scan in the dark to high voltage values, LSV experiment with varying CdS thicknesses, EQE, SEM, and EDS of different sulfides, and Gaussian fits to the XRD spectra of $Cd_xZn_{1-x}S$ solid solutions. This material is available free of charge via the Internet at http://pubs.acs.org.

AUTHOR INFORMATION

Corresponding Author

*E-mail: mokari@bgu.ac.il.

Notes

The authors declare no competing financial interest.

ACKNOWLEDGMENTS

This work was supported by the European Research Council (ERC), starting grant, Project 278779. Part of this research was conducted as part of the framework of the Energy Initiative Program and partially supported by the Adelis Foundation for renewable energy research. M.V. thanks the Merage Foundation for financial support. We thank Dr. Vladimir Ezersky for high-resolution and analytical TEM and Dr. Anna Milionshchik for TGA.

REFERENCES

(1) Kim, H.; Jeong, H.; An, T. K.; Park, C. E.; Yong, K. Hybrid-Type Quantum-Dot Cosensitized ZnO Nanowire Solar Cell with Enhanced Visible-Light Harvesting. *ACS Appl. Mater. Interfaces* **2013**, *5*, 268−275.

(2) Jean, J.; Chang, S.; Brown, P. R.; Cheng, J. J.; Rekemeyer, P. H.; Bawendi, M. G.; Gradečak, S.; Bulović, V. ZnO Nanowire Arrays for Enhanced Photocurrent in PbS Quantum Dot Solar Cells. *Adv. Mater.* **2013**, *25*, 2790−2796.

(3) Edri, E.; Cohen, H.; Hodes, G. Band Alignment in Partial and Complete ZnO/ZnS/CdS/CuSCN Extremely Thin Absorber Cells: An X-Ray Photoelectron Spectroscopy Study. *ACS Appl. Mater. Interfaces* **2013**, *5*, 5156−5164.

(4) Chen, H. M.; Chen, C. K.; Liu, R.-S.; Wu, C.-C.; Chang, W.-S.; Chen, K.-H.; Chan, T.-S.; Lee, J.-F.; Tsai, D. P. A New Approach to Solar Hydrogen Production: A ZnO-ZnS Solid Solution Nanowire Array Photoanode. *Adv. Energy Mater.* **2011**, *1*, 742−747.

(5) Chen, H. M.; Chen, C. K.; Lin, C. C.; Liu, R.-S.; Yang, H.; Chang, W.-S.; Chen, K.-H.; Chan, T.-S.; Lee, J.-F.; Tsai, D. P. Multi-Bandgap-Sensitized ZnO Nanorod Photoelectrode Arrays for Water Splitting: An X-ray Absorption Spectroscopy Approach for the Electronic Evolution under Solar Illumination. *J. Phys. Chem. C* **2011**, *115*, 21971−21980.

(6) Miao, J.; Yang, H. B.; Khoo, S. Y.; Liu, B. Electrochemical Fabrication of ZnO-CdSe Core-Shell Nanorod Arrays for Efficient Photoelectrochemical Water Splitting. *Nanoscale* **2013**, *5*, 11118−11124.

(7) Li, N.; Zhou, B.; Guo, P.; Zhou, J.; Jing, D. Fabrication of Noble-Metal-Free $Cd_{0.5}Zn_{0.5}S$/NiS Hybrid Photocatalyst for Efficient Solar Hydrogen Evolution. *Int. J. Hydrogen Energy* **2013**, *38*, 11268−11277.

(8) Tak, Y.; Kim, H.; Lee, D.; Yong, K. Type-II CdS Nanoparticle-ZnO Nanowire Heterostructure Arrays Fabricated by a Solution

Process: Enhanced Photocatalytic Activity. *Chem. Commun.* **2008**, 4585−4587.
(9) Xia, X.; Tu, J.; Zhang, Y.; Wang, X.; Gu, C.; Zhao, X.-B.; Fan, H. J. High-Quality Metal Oxide Core/Shell Nanowire Arrays on Conductive Substrates for Electrochemical Energy Storage. *ACS Nano* **2012**, *6*, 5531−5538.
(10) Lu, M.-Y.; Song, J.; Lu, M.-P.; Lee, C.-Y.; Chen, L.-J.; Wang, Z. L. ZnO-ZnS Heterojunction and ZnS Nanowire Arrays for Electricity Generation. *ACS Nano* **2009**, *3*, 357−362.
(11) Tian, W.; Zhang, C.; Zhai, T.; Li, S.-L.; Wang, X.; Liu, J.; Jie, X.; Liu, D.; Liao, M.; Koide, Y.; Golberg, D.; Bando, Y. Flexible Ultraviolet Photodetectors with Broad Photoresponse Based on Branched ZnS-ZnO Heterostructure Nanofilms. *Adv. Mater.* **2014**, *26*, 3088−3093.
(12) Zhai, J.; Wang, L.; Wang, D.; Li, H.; Zhang, Y.; He, D. Q.; Xie, T. Enhancement of Gas Sensing Properties of CdS Nanowire/ZnO Nanosphere Composite Materials at Room Temperature by Visible-Light Activation. *ACS Appl. Mater. Interfaces* **2011**, *3*, 2253−2258.
(13) Zirak, M.; Akhavan, O.; Moradlou, O.; Nien, Y. T.; Moshfegh, A. Z. Vertically Aligned ZnO@CdS Nanorod Heterostructures for Visible Light Photoinactivation of Bacteria. *J. Alloys Compd.* **2014**, *590*, 507−513.
(14) Ramasamy, K.; Malik, M. A.; O'Brien, P.; Raftery, J. Metal Complexes of Thiobiurets and Dithiobiurets: Novel Single Source Precursors for Metal Sulfide Thin Film Nanostructures. *Dalton Trans.* **2010**, *39*, 1460−1463.
(15) Ramasamy, K.; Kuznetsov, V. L.; Gopal, K.; Malik, M. A.; Raftery, J.; Edwards, P. P.; O'Brien, P. Organotin Dithiocarbamates: Single-Source Precursors for Tin Sulfide Thin Films by Aerosol-Assisted Chemical Vapor Deposition (AACVD). *Chem. Mater.* **2013**, *25*, 266−276.
(16) Ramasamy, K.; Malik, M. A.; O'Brien, P.; Raftery, J. The Synthesis and Structure of a Cadmium Complex of Dimorpholinodithioacetylacetonate and Its Use as Single Source Precursor for CdS Thin Films or Nanorods. *Dalton Trans.* **2009**, 2196−2200.
(17) Barreca, D.; Gasparotto, A.; Maragno, C.; Tondello, E. CVD of Nanosized ZnS and CdS Thin Films from Single-Source Precursors. *J. Electrochem. Soc.* **2004**, *151*, G428−G435.
(18) O'Brien, P.; Waters, J. Deposition of Ni and Pd Sulfide Thin Films via Aerosol-Assisted CVD. *Chem. Vap. Deposition* **2006**, *12*, 620−626.
(19) Frigo, D. M.; Khan, O. F. Z.; O'Brien, P. Growth of Epitaxial and Highly Oriented Thin Films of Cadmium and Cadmium Zinc Sulfide by Low-Pressure Metalorganic Chemical Vapour Deposition Using Diethyldithiocarbamates. *J. Cryst. Growth* **1989**, *96*, 989−992.
(20) Fainer, N. I.; Kosinova, M. L.; Rumyantsev, Y. M.; Salman, E. G.; Kuznetsov, F. A. Growth of PbS and CdS Thin Films by Low-Pressure Chemical Vapour Deposition Using Dithiocarbamates. *Thin Solid Films* **1996**, *280*, 16−19.
(21) Nomura, R.; Miyawaki, K.; Toyosaki, T.; Matsuda, H. Preparation of Copper Sulfide Thin Layers by a Single-Source MOCVD Process. *Chem. Vap. Deposition* **1996**, *2*, 174−179.
(22) Sengupta, S. K.; Kumar, S. Thermal Studies on Metal Dithiocarbamato Complexes. A Review. *Thermochim. Acta* **1984**, *72*, 349−361.
(23) Honjo, T.; Imura, H.; Shima, S.; Kiba, T. Vacuum Sublimation Behavior of Various Metal Chelates of 4-Anilino-3-Pentene-2-One, Acetylacetone, Dithiocarbamates, Oxine and Its Derivatives, Dimethylglyoxime, Dithizone, 1-(2-Pyridylazo)-2-naphthol, and Tetraphenylporphyrin. *Anal. Chem.* **1978**, *50*, 1545−1552.
(24) Trindade, T.; O'Brien, P. Synthesis of CdS and CdSe Nanoparticles by Thermolysis of Diethyldithio- or Diethyldiseleno-Carbamates of Cadmium. *J. Mater. Chem.* **1996**, *6*, 343−347.
(25) Jen-La Plante, I.; Zeid, T. W.; Yang, P.; Mokari, T. Synthesis of Metal Sulfide Nanomaterials via Thermal Decomposition of Single-Source Precursors. *J. Mater. Chem.* **2010**, *20*, 6612−6617.
(26) Sun, J.; Buhro, W. E. The Use of Single-Source Precursors for the Solution−Liquid−Solid Growth of Metal Sulfide Semiconductor Nanowires. *Angew. Chem.* **2008**, *120*, 3259−3262.
(27) Rukenstein, P.; Jen-La Plante, I.; Diab, M.; Chockler, E.; Flomin, K.; Moshofsky, B.; Mokari, T. Selective Growth of Metal Sulfide Tips onto Cadmium Chalcogenide Nanostructures. *CrystEngComm* **2012**, *14*, 7590−7593.
(28) Barrelet, C. J.; Wu, Y.; Bell, D. C.; Lieber, C. M. Synthesis of CdS and ZnS Nanowires Using Single-Source Molecular Precursors. *J. Am. Chem. Soc.* **2003**, *125*, 11498−11499.
(29) Dasgupta, N. P.; Jung, H. J.; Trejo, O.; McDowell, M. T.; Hryciw, A.; Brongersma, M.; Sinclair, R.; Prinz, F. B. Atomic Layer Deposition of Lead Sulfide Quantum Dots on Nanowire Surfaces. *Nano Lett.* **2011**, *11*, 934−940.
(30) Myung, Y.; Jang, D. M.; Sung, T. K.; Sohn, Y. J.; Jung, G. B.; Cho, Y. J.; Kim, H. S.; Park, J. Composition-Tuned ZnO-CdSSe Core-Shell Nanowire Arrays. *ACS Nano* **2010**, *4*, 3789−3800.
(31) Sulieman, K. M.; Huang, X.; Liu, J.; Tang, M. One-Step Growth of ZnO/ZnS Core−Shell Nanowires by Thermal Evaporation. *Smart Mater. Struct.* **2007**, *16*, 89−92.
(32) Jin, M.-J.; Chen, X.-Y.; Gao, Z.-M.; Ling, T.; Du, X.-W. Improve Photo-Electron Conversion Efficiency of ZnO/CdS Coaxial Nanorods by P-Type CdTe Coating. *Nanotechnology* **2012**, *23*, 485401.
(33) Hwang, I.; Yong, K. Environmentally Benign and Efficient Ag_2S-ZnO Nanowires as Photoanodes for Solar Cells: Comparison with CdS-ZnO Nanowires. *ChemPhysChem* **2013**, *14*, 364−368.
(34) Wang, H.; Kubo, T.; Nakazaki, J.; Kinoshita, T.; Segawa, H. PbS-Quantum-Dot-Based Heterojunction Solar Cells Utilizing ZnO Nanowires for High External Quantum Efficiency in the Near-Infrared Region. *J. Phys. Chem. Lett.* **2013**, *4*, 2455−2460.
(35) Le Bahers, T.; Rérat, M.; Sautet, P. Semiconductors Used in Photovoltaic and Photocatalytic Devices: Assessing Fundamental Properties from DFT. *J. Phys. Chem. C* **2014**, *118*, 5997−6008.
(36) Diab, M.; Volokh, M.; Moshofsky, B.; Jen-La Plante, I.; Flomin, K.; Chockler, E.; Mokari, T. A Simple Approach for the Formation of Oxides, Sulfides, and Oxide-Sulfide Hybrid Nanostructures. *Isr. J. Chem.* **2012**, *52*, 1081−1089.
(37) Khan, O. F. Z.; O'Brien, P. Synthesis, Characterization, ^{113}Cd NMR and Decomposition of Some Cadmium Thiolates. *Polyhedron* **1991**, *10*, 325−332.
(38) Srikant, V.; Clarke, D. R. On the Optical Band Gap of Zinc Oxide. *J. Appl. Phys.* **1998**, *83*, 5447−5451.
(39) Weller, H. Colloidal Semiconductor Q-Particles: Chemistry in the Transition Region Between Solid State and Molecules. *Angew. Chem., Int. Ed.* **1993**, *32*, 41−53.
(40) Chen, H. M.; Chen, C. K.; Liu, R.-S.; Zhang, L.; Zhang, J.; Wilkinson, D. P. Nano-Architecture and Material Designs for Water Splitting Photoelectrodes. *Chem. Soc. Rev.* **2012**, *41*, 5654−5671.
(41) Zhao, Y.; Zhang, Y.; Zhu, H.; Hadjipanayis, G. C.; Xiao, J. Q. Low-Temperature Synthesis of Hexagonal (Wurtzite) ZnS Nanocrystals. *J. Am. Chem. Soc.* **2004**, *126*, 6874−6875.
(42) Fedorov, V. A.; Ganshin, V. A.; Korkishko, Y. N. Solid-State Phase Diagram of the Zinc Sulfide-Cadmium Sulfide System. *Mater. Res. Bull.* **1993**, *28*, 59−66.
(43) Dachraoui, M.; Vedel, J. Sprayed CdS-Cu_2S Solar Cells: Structural and Chemical Properties of Airless Sprayed CdS and CdZnS Layers. *Sol. Cells* **1985**, *15*, 319−327.